

Article

Synthesis of *N*-Substituted Pyrroles Catalyzed by Low-Cost and Commercially Available Aluminas

Omar Portilla-Zúñiga ¹, Óscar M. Bautista-Aguilera ², José J. Martínez ³, Hugo Rojas ³, Mario A. Macías ⁴, Isabel Iriepa ^{2,5}, Adrián Pérez-Redondo ^{2,5}, Ángel Sathicq ^{1,*}, Juan-Carlos Castillo ^{3,*} and Gustavo P. Romanelli ^{1,6}

- ¹ Centro de Investigación y Desarrollo en Ciencias Aplicadas “Dr. Jorge J. Ronco” (CINDECA-CCT La Plata-CONICET-CIC-PBA), Universidad Nacional de La Plata, Calle 47 No. 257, La Plata B1900AJK, Argentina
 - ² Departamento de Química Orgánica y Química Inorgánica, Ctra. Madrid-Barcelona, Universidad de Alcalá, Km. 33, 6, 28871 Madrid, Spain
 - ³ Escuela de Ciencias Químicas, Universidad Pedagógica y Tecnológica de Colombia, Avenida Central del Norte 39-115, Tunja 150003, Colombia
 - ⁴ Crystallography and Chemistry of Materials, Department of Chemistry, Universidad de los Andes, Carrera 1 No. 18A-10, Bogotá 111711, Colombia
 - ⁵ Institute of Chemical Research Andrés M. del Río, Universidad de Alcalá, Alcalá de Henares, 28805 Madrid, Spain
 - ⁶ Centro de Investigación en Sanidad Vegetal (CISaV)/Cátedra de Química Orgánica, Facultad de Ciencias Agrarias y Forestales, Universidad Nacional de La Plata, Calles 60 y 119 s/n, La Plata B1904AAN, Argentina
- * Correspondence: agsathicq@quimica.unlp.edu.ar (Á.S.); juan.castillo06@uptc.edu.co (J.-C.C.); Tel.: +54-221-421-1353 (Á.S.); +57-8-740-5626 (ext. 2425) (J.-C.C.)

Abstract: The Paal-Knorr reaction of acetylacetone with primary amines catalyzed by CATAPAL 200 under conventional heating at 60 °C for 45 min afforded *N*-substituted pyrroles in 68–97% yields. The pyrrole **3g** was studied by single-crystal and powder X-ray diffraction. The high percentage of Brønsted–Lewis acid sites (23%) and pore diameter (37.8 nm) of CATAPAL 200 favor the formation of the pyrrole ring because an increase in Brønsted acid sites efficiently catalyzes condensation and dehydration processes. This protocol is distinguished by its operational simplicity, high yields, reduced reaction time, no solvent required, stoichiometric amounts of reactants, low catalyst loading, and clean reaction profile. In addition, the CATAPAL 200 is cheap and commercially available leading to an efficient and lower-cost chemical transformation. The reusability of the catalyst for up to five cycles without appreciable loss of its catalytic activity makes the present protocol sustainable and advantageous compared to conventional methods.

Keywords: pyrroles; aluminas; heterogeneous catalysis; Paal-Knorr reaction; green chemistry; X-ray crystallography



Citation: Portilla-Zúñiga, O.; Bautista-Aguilera, Ó.M.; Martínez, J.J.; Rojas, H.; Macías, M.A.; Iriepa, I.; Pérez-Redondo, A.; Sathicq, Á.; Castillo, J.-C.; Romanelli, G.P. Synthesis of *N*-Substituted Pyrroles Catalyzed by Low-Cost and Commercially Available Aluminas. *Catalysts* **2023**, *13*, 603. <https://doi.org/10.3390/catal13030603>

Academic Editors: Victorio Cadierno and Raffaella Mancuso

Received: 9 February 2023

Revised: 8 March 2023

Accepted: 13 March 2023

Published: 16 March 2023



Copyright: © 2023 by the authors. Licensee MDPI, Basel, Switzerland. This article is an open access article distributed under the terms and conditions of the Creative Commons Attribution (CC BY) license (<https://creativecommons.org/licenses/by/4.0/>).

1. Introduction

The pyrrole is a five-membered *N*-heteroaromatic compound containing one nitrogen atom. Currently, synthetic and naturally occurring pyrrole derivatives have attracted considerable attention due to their broad range of pharmaceutical and biological properties [1–3], proving to be significant structural components of active pharmaceutical ingredients (APIs) and bioactive pyrrole-based compounds. The pyrrole moiety is widely distributed in nature, forming part of heterocyclic macrocycles such as porphyrins, chlorophyll, heme, vitamin B12, and pigments [4]. Moreover, FDA-approved drugs containing the pyrrole scaffold have been developed. For instance, Ketorolac is used for the short-term treatment of moderate to severe pain [5], Sunitinib is employed to treat certain types of cancer [6], Atorvastatin is a Hydroxymethylglutaryl-CoA (HMG-CoA) reductase inhibitor used to reduce the levels of LDL cholesterol [7], the antiviral agent Remdesivir is a promising drug for the treatment of patients affected by COVID-19, among other marketed drugs

(Figure 1) [8]. Due to the structural diversity of pyrrole derivatives in the therapeutic response profile, many researchers have been working on exploring this skeleton against several diseases and disorders. Since pyrroles are valuable building blocks in medicinal chemistry and drug design, their synthesis by simple, efficient, and eco-friendly procedures is highly desirable in modern organic synthesis [9–12]. Among the arsenal of procedures to obtain pyrroles, the most classic methods involve the Hantzsch reaction [13], the Knorr reaction [14], and the Paal-Knorr reaction [15], which involves the condensation of γ -diketones with primary amines (or ammonia) by an acid-mediated dehydrative cyclization.

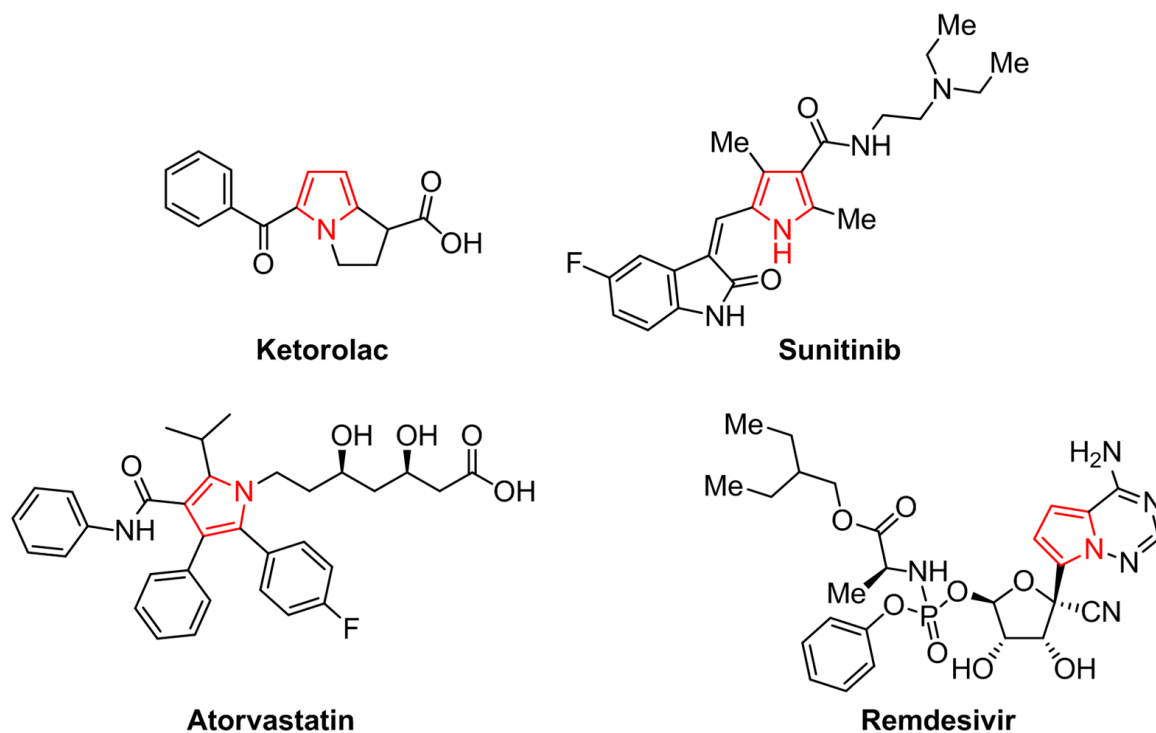


Figure 1. Relevant pyrrole-based drugs approved by the FDA.

A broad scope of catalysts based on Brønsted acids have been employed in the Paal-Knorr synthesis, including acetic acid [16], phosphoric acid [17], sulfamic acid [18], *p*-toluenesulfonic acid [19], among others [15]. Alternative methods based on solid acid catalysts offer major advantages over Brønsted acids. For instance, the use of clays such as montmorillonite KSF and Fe(III)-montmorillonite displayed a high catalytic activity for the synthesis of pyrroles in 69–96% yields in the presence of dichloromethane at room temperature for 1–25 h [20]. Alternatively, acids bound to a variety of support materials lead to short reaction times, simple workup, and better catalyst recovery. For instance, sulfonated heterogeneous catalysts such as silica sulfuric acid, dendritic amine grafted on mesoporous silica, cellulose sulfuric acid, and sulfonic acid grafted onto polyethylene glycol 400-encapsulated Fe₃O₄ nanoparticles catalyzed the solvent-free synthesis of pyrroles in 70–99% yields at room temperature for 3–120 min [20].

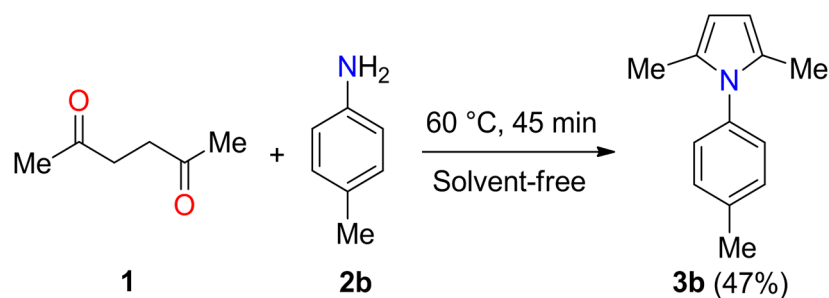
Lewis acid catalysts showed remarkable performances on the broad scope of pyrrole derivatives. In particular, the use of eco-friendly protocols catalyzed by metal halides such as FeCl₃ [21], CaCl₂ [22], RuCl₃ [23], CoCl₂ [24], InCl₃ or InBr₃ [25], ZrCl₄ [26], ZrOCl₂·8H₂O [27], CuI/C [28], and MgI₂ [29], among others, have been reported for this purpose. For instance, Aghapoor and colleagues described the use of CaCl₂·2H₂O (20 mol %) for the synthesis of *N*-substituted pyrroles in 74–97% yields in an open vessel and irradiated at 420 W (70% of maximum power) for 10 min [22]. Alternatively, metal chlorides deposited on supports improved the yields of pyrrole derivatives. For instance, Rahmatpour described the use of polystyrene-supported aluminum trichloride (PS/AlCl₃,

15 mol %) and gallium trichloride (PS/GaCl₃, 10 mol %) as efficient and reusable heterogeneous Lewis acid catalysts for the synthesis of *N*-substituted pyrroles in 83–95% and 83–97% yields for 30–135 min and 8–45 min, respectively, under refluxing acetonitrile [30,31]. These protocols have the advantages of the reusability and stability of the catalyst, operational simplicity, and simple workup procedure. In addition, silica-supported bismuth(III) chloride (BiCl₃/SiO₂, 7.5 mol %) and antimony(III) chloride (SbCl₃/SiO₂, 10 mol %) have been employed as efficient and reusable heterogeneous Lewis acid catalysts for the synthesis of *N*-substituted pyrroles in 22–96% and 51–94% yields for 60 min, respectively, stirring in hexane at ambient temperature [32,33]. The investigation of different oxide surfaces displayed that 40 mg of nanoporous silica MCM-41 (1500 m²g⁻¹) catalyzes the solvent-free Paal-Knorr reaction leading to *N*-substituted pyrroles in 73–95% yields at 70 °C for 25–240 min, which is due to a significantly higher surface area than silica gel SiO₂ (400 m²g⁻¹) [34].

The use of support increases the available metal surface area making the catalyst more mechanically robust and catalytically active because it stabilizes the active species [35]. In some cases, the support can introduce new active sites, which are usually acidic, basic, or both, leading to a bifunctional catalyst. However, supported metal catalysts are susceptible to poisoning by molecules containing sulfur, nitrogen, chlorine, and oxygen, even at low concentrations [35]. Among them, alumina is extensively used as a support due to its high mechanical strength, surface area, thermal stability, and low cost of production [36]. In addition, alumina is employed as a catalyst in different chemical transformations because its surface contains acidic and basic sites [37,38]. However, the use of this inexpensive inorganic solid has been scarcely explored to condense primary amines with γ -diketones. In this regard, we recently reported the use of Preyssler heteropolyacids supported on mesoporous alumina as bifunctional catalysts for the Paal-Knorr synthesis of pyrrole derivatives in 50–98% yields at 60 °C for 30–180 min under solvent-free conditions [39]. Although heteropolyacid-based materials have strong Brønsted acidity and high thermal and hydrolytic stability, they are generally synthesized by complex procedures. Thus, the interest has increased in developing procedures for this reaction that include the principles of green chemistry and the use of straightforward, cheap, and reusable catalysts. Herein, we report a solvent-free procedure for the Paal-Knorr synthesis of *N*-substituted pyrroles in good yields and high selectivity using commercially available, cheap, and reusable aluminas supplied by SASOL Company.

2. Results and Discussion

The Paal-Knorr reaction of acetonylacetone **1** with 4-toluidine **2b** at 60 °C for 45 min under solvent-free conditions was studied using commercially available aluminas (SASOL). In a blank experiment, the 2,5-dimethyl-1-(4-tolyl)-1*H*-pyrrole **3b** was obtained in 47% yield in the absence of catalyst (Scheme 1). As shown in Table 1, the use of CATAPAL C-1, CATALOX Sba-90, and CATALOX Sba-200 lead to the corresponding product **3b** in 58%, 64%, and 46% yields, respectively. Surprisingly, the catalyst CATAPAL 200 afforded 2,5-dimethyl-1-(4-tolyl)-1*H*-pyrrole **3b** in 96% yield. The aluminas were characterized by powder X-ray diffraction, N₂-physisorption, and measurement of acidity to explain this unexpected result.



Scheme 1. Paal-Knorr synthesis of 2,5-dimethyl-1-(4-tolyl)-1*H*-pyrrole **3b**.

Table 1. Paal-Knorr synthesis of pyrrole **3b** and characterization of commercially available aluminas supplied by company SASOL ^a.

Entry	Catalyst	Yield 3b (%)	IEP ^b (mV)	L (%) ^c	B–L (%) ^c	S _{BET} (m ² g ^{−1})	PD (nm) ^d	PV (cm ³ g ^{−1}) ^e
1	– ^f	47	–	–	–	–	–	–
2	CATAPAL 200	96	23.7	77	23	47	37.8	0.44
3	CATAPAL C-1	58	−5.6	80	20	239	6.3	0.37
4	CATALOX SBA-90	64	58.0	88	12	107	14.6	0.39
5	CATALOX SBA-200	46	45.3	92	8	199	8.4	0.42

^a Reaction conditions: acetylacetone **1** (1 mmol), 4-toluidine **2b** (1 mmol), and 40 mg of the catalyst at 60 °C for 45 min under solvent-free conditions. The product was purified by flash column chromatography and purity control by GC. ^b Initial electrode potential was obtained by potentiometric titration with *n*-butylamine. ^c Percentage of Lewis (L) and Brønsted–Lewis (B–L) acid sites obtained from pyridine adsorption followed by FT-IR. ^d Pore diameter (PD) is an average pore width determined by N₂-physisorption at 77 K. ^e Pore volume (PV). ^f Absence of catalyst.

Powder X-ray diffraction evidenced that CATAPAL-type aluminas show characteristic peaks of the boehmite, while CATALOX-type aluminas display peaks of the γ -Al₂O₃ phase. Among them, the catalytic behavior was very different. In particular, CATAPAL 200 afforded the desired product in higher yield than CATAPAL C-1, which could be associated with a better crystallinity of the boehmite. According to the surface area, the aluminas present broad differences. However, the pore diameter shows a linear trend with the yield (Table 1). The formation of **3b** could be favored with a greater pore diameter to facilitate the desorption process, which is supported by a change in color and an increase in the weight of catalysts with smaller pores. Thus, CATAPAL C-1 and CATALOX SBA-200 aluminas with the smallest pore diameters generated the lowest yields (Table 1). In summary, the catalytic activity of commercially available and inexpensive aluminas could be related to the pore diameter.

On the other hand, the presence of Lewis acid sites was evidenced through FT-IR spectroscopy analysis by pyridine adsorption (Table 1). Moreover, some Brønsted–Lewis acid sites were detected in a minor proportion. Overall, CATAPAL-type aluminas have lower Lewis acid sites and higher Brønsted–Lewis acid sites than CATALOX-type aluminas. Although an increase in the Lewis acid sites diminished the catalytic activity of aluminas, the highest percentage of Brønsted–Lewis acid sites and pore diameter generated the best yield of **3b**. It should be noted that an increase in Brønsted acid sites could play a key role in the dehydration step.

Afterward, the effect of catalyst mass was studied in the Paal-Knorr reaction at 60 °C for 45 min using CATAPAL 200. As shown in Table 2, a directly proportional behavior between catalyst mass and yield is observed. However, duplicating the catalyst mass from 40 to 80 mg slightly decreases the yield of **3b**. In all cases, unwanted products were observed by TLC [40,41]. Thus, 40 mg of catalyst mass was chosen as the optimal amount to evaluate the generality of the scope of this Paal-Knorr reaction.

Table 2. Effect of amount of catalyst on pyrrole **3b** yield.

Entry	Catalyst Mass (mg)	Yield 3b (%) ^a
1	0	47
2	4	55
3	10	58
4	20	80
5	40	96
6	80	90

^a Reaction conditions: acetylacetone **1** (1 mmol) and 4-toluidine **2b** (1 mmol) at 60 °C for 45 min under solvent-free conditions. The product was purified by column chromatography.

Next, the Paal-Knorr reaction was studied with 40 mg of catalyst at five temperature intervals between 20 and 100 °C for 45 min. As shown in Table 3, the best yield of pyrrole **3b** was reached at 60 °C (Table 3, Entry 3). Strangely, the use of temperatures higher than 60 °C did not improve the yield of **3b** (Table 3, entries 4 and 5). Although a condensation reaction occurred rapidly at high temperatures, we observed that yields diminish at 80 and 100 °C possibly due to the formation of unwanted products such as 3-hydroxy-3-methylcyclopentanone [40], 3-methyl-2-cyclopenten-1-one [40], or 2,5-dimethylfuran [41], which are formed via an intramolecular aldol reaction of the acetylacetone. Unfortunately, we do not have experimental data to confirm the structures of these by-products.

Table 3. Effect of temperature on pyrrole **3b** yield.

Entry	Temperature (°C)	Yield 3b (%) ^a
1	20	10
2	40	40
3	60	96
4	80	80
5	100	67

^a Reaction conditions: acetylacetone **1** (1 mmol), 4-toluidine **2b** (1 mmol), and catalyst (40 mg) for 45 min under solvent-free conditions. The product was purified by column chromatography.

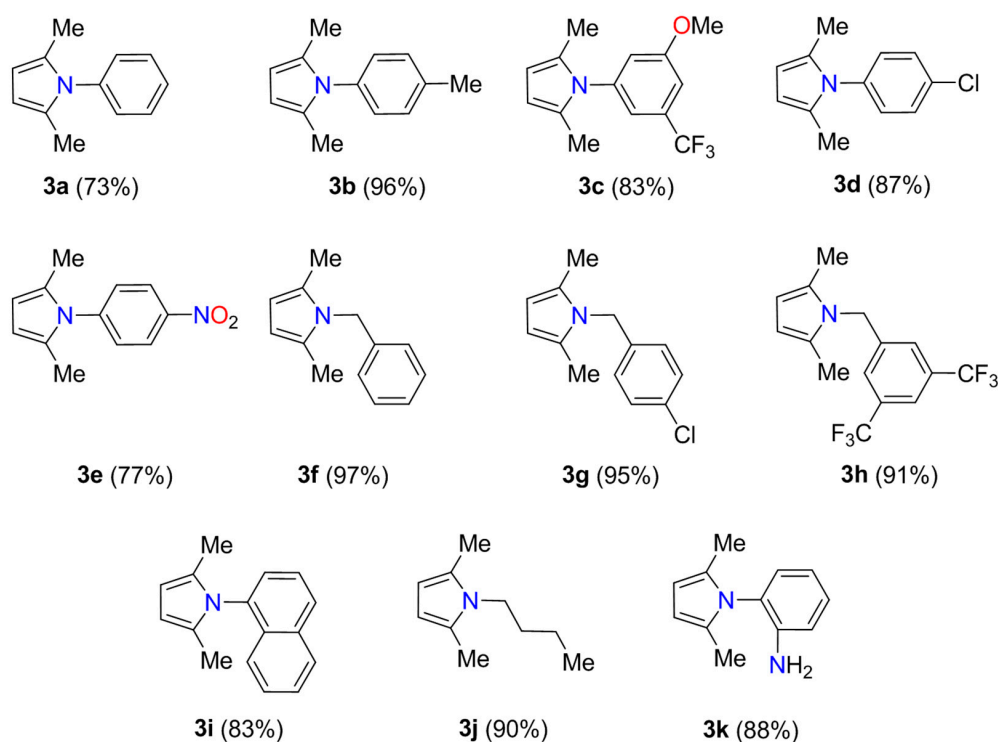
In the next step, the effect of time on pyrrole yield was investigated using four time intervals from 30 to 120 min at 60 °C with 40 mg of catalyst (Table 4). In summary, the Paal-Knorr reaction proceeds in excellent yields employing times of 45 and 60 min (Table 4, Entries 2 and 3). When the reaction was performed employing times greater than 60 min, the yield decreased by approximately 16%, which could be explained by the formation of unidentified by-products [40,41]. Therefore, the optimal time is 45 min because it leads to the best yield of pyrrole **3b**. To our delight, this protocol fulfills at least 8 out of the 12 principles of Green Chemistry, including (1) prevention, (2) atom economy, (3) less hazardous chemical syntheses, (4) designing safer chemicals, (5) safer solvents and auxiliaries, (6) reduced derivatives, (7) catalysis, and (8) inherently safer chemistry for accident prevention.

Table 4. Effect of time on pyrrole **3b** yield.

Entry	Time (min)	Yield 3b (%) ^a
1	30	52
2	45	96
3	60	96
4	120	80

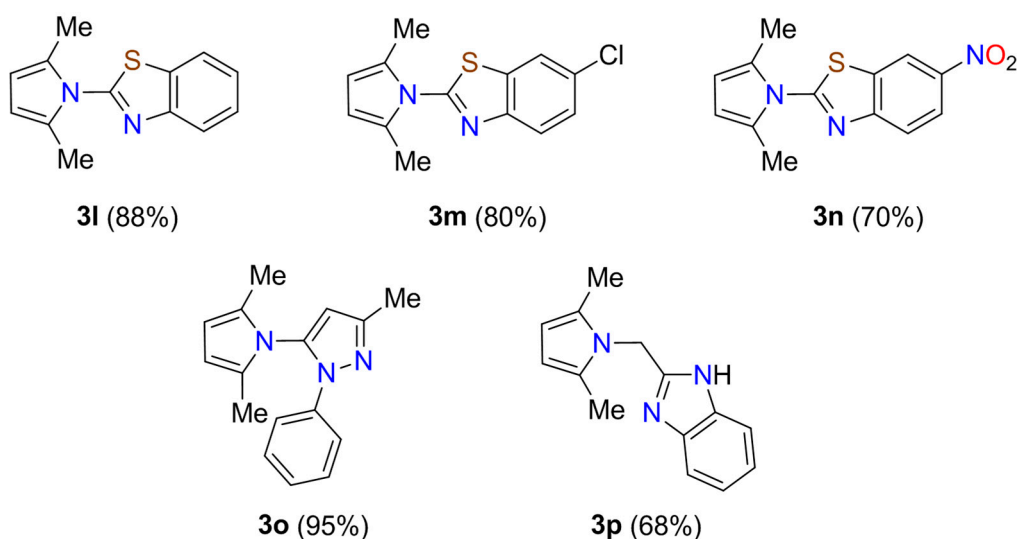
^a Reaction conditions: acetylacetone **1** (1 mmol), 4-toluidine **2b** (1 mmol), and catalyst (40 mg) at 60 °C under solvent-free conditions. The product was purified by column chromatography.

We next investigated the generality and limitations of the Paal-Knorr reaction catalyzed by CATAPAL 200 (40 mg) at 60 °C for 45 min. In all cases, pyrrole derivatives **3a–p** were obtained in good to excellent yields (68–97%) and selectivity close to 100% after purification by column chromatography. Initially, the reaction of acetylacetone **1** with aniline derivatives **2a–e** afforded *N*-arylpyrroles **3a–e** in 73–96% yields (Scheme 2). No loss of efficacy was observed for electron-withdrawing (i.e., 5-CF₃, 4-Cl, and 4-NO₂) and electron-donating (i.e., 4-Me and 3-MeO) groups attached to the benzene ring. Afterward, the generality of this reaction was studied with benzylamine derivatives **2f–h** leading to pyrrole derivatives **3f–h** in 91–97% yields. The reaction was also conducted with 1-naphthylamine and *n*-butylamine to afford pyrrole derivatives in good yields. Remarkably, the *o*-phenylenediamine **2k** selectively reacted at just one of the amino groups with acetylacetone **1** to furnish **3k** in 88% yield.



Scheme 2. Paal-Knorr synthesis of *N*-substituted pyrroles **3a–k**.

We then examined the synthesis of pyrrole-based *N*-heterocycles starting from amino-*N*-heterocycles to demonstrate the power of the C–N bond formation. The synthesis was initiated by the Paal-Knorr reaction of acetylacetone **1** with diverse benzo[*d*]thiazol-2-amines **2l–n** to provide pyrrole-benzothiazole hybrids **3l–n** in 70–88% yields (Scheme 3). As a further application, this protocol is successfully extended to 3-methyl-1-phenyl-1*H*-pyrazol-5-amine **2o** and (1*H*-benzo[*d*]imidazol-2-yl)methanamine **2p** to afford new pyrrole derivatives **3o** and **3p** in 95% and 68% yields, respectively, which could be used as building blocks in the synthesis of more complex structures and pharmaceutically active molecules. Overall, this protocol is distinguished by its operational simplicity, high yielding, reduced reaction time, high atom economy, environmental friendliness, and clean reaction profile.



Scheme 3. Paal-Knorr synthesis of pyrrole-based *N*-heterocycles **3l–p**.

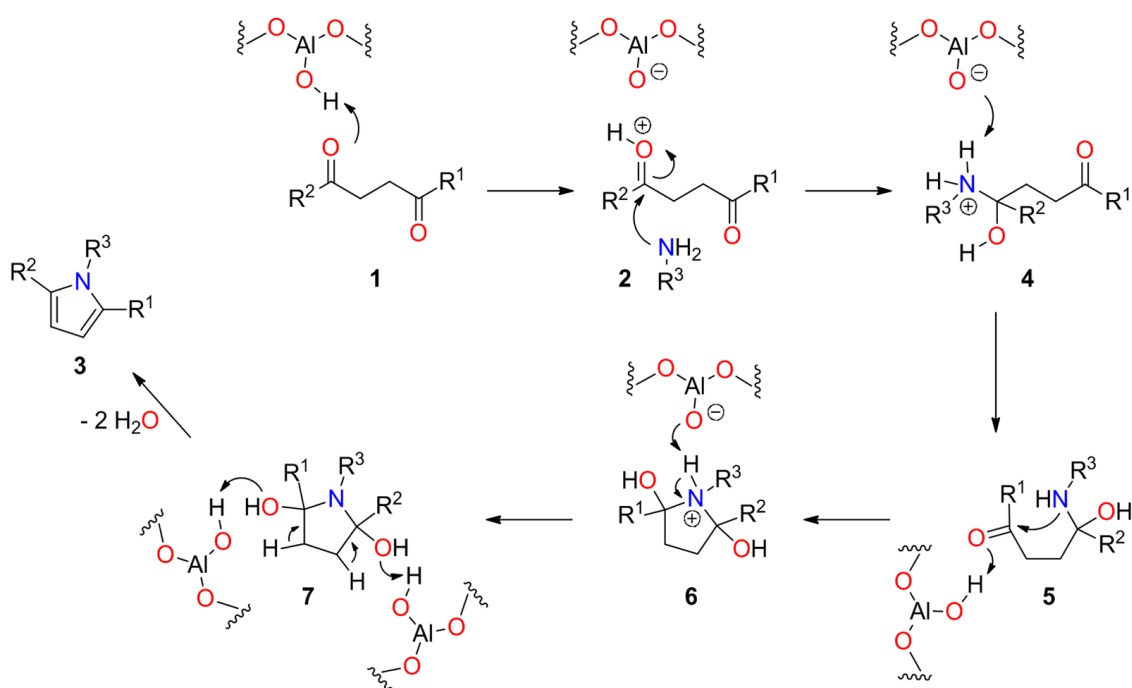
Due to the importance of heterogeneous catalysts in industrial processes, we investigated the recyclability of the CATAPAL 200 in five run reactions for obtaining pyrrole **3b** under the optimized conditions (Table 5). After each reaction cycle, the product was extracted with ethyl acetate (2×5 mL), and the catalyst was separated by centrifugation and filtration. Afterward, the catalyst was washed with toluene (2×1 mL), ethanol (2×1 mL), and dried under vacuum. As shown in Table 5, the yield of pyrrole **3b** only decreased by 8% after five catalytic cycles, confirming the noteworthy stability and applicability of this solid in the solvent-free Paal-Knorr reaction. A darkening of the recovered catalyst is observed due to the decomposition of organic species; however, no weight loss is detected after five catalytic cycles.

Table 5. Catalyst recycling capability in the synthesis of pyrrole **3b** under optimized conditions.

Entry	Reuse Cycle	Yield 3b (%) ^a
1	1	96
2	2	94
3	3	90
4	4	90
5	5	88

^a Reaction conditions: acetonylacetone **1** (1 mmol), 4-toluidine **2b** (1 mmol), and catalyst (CATAPAL 200, 40 mg) at 60 °C for 45 min under solvent-free conditions. The product was purified by column chromatography.

γ -Alumina has been extensively used as a support for preparing diverse heterogeneous catalysts as well as a binder for zeolite-type materials employed in fluid catalytic cracking (FCC) due to its physical performances and acidity for pre-cracking of hydrocarbon macromolecules. Traditional γ -alumina possesses only Lewis acidity that causes severe coke formation [42,43]. Thus, an innovative idea is to reduce Lewis acidity and/or generate more Brønsted acidic sites by surface modification of γ -alumina to decrease the coke formation [42,43]. In this sense, CATAPAL 200 has rich Brønsted acid sites and reduced Lewis acid sites (Table 1, Entry 2). Thus, we hypothesize that Brønsted acid sites favor the formation of pyrroles **3** in good yields, high selectivity, and short reaction times under mild reaction conditions. The plausible mechanism for the synthesis of *N*-substituted pyrroles **3** involves a sequence of chemical reactions occurring in a single step (Scheme 4). It begins with the protonation of the oxygen atom of one carbonyl group of **1** by Brønsted acid sites of the catalyst, and subsequent nucleophilic attack of the amine group of **2** to afford intermediate **4**. Then, the abstraction of the proton from intermediate **4** regenerates the catalyst and results in the γ -aminoketone **5**, which suffers an intramolecular nucleophilic attack of the amine group on the second carbonyl group activated by Brønsted acid sites of the catalyst leading to intermediate **6**. Finally, the Brønsted acid-catalyzed dehydration of pyrrolidine-2,5-diol **7** affords pyrrole ring and two molecules of water. We concluded that the CATAPAL 200 catalyzes key steps during the formation of the pyrrole ring due to its rich Brønsted acid sites, which was confirmed by the percentage of Brønsted–Lewis (B–L, 23%) acid sites (Table 1, Entry 2). In this sense, some authors have reported that Lewis acid sites predominate on dehydrated silica–alumina; however, the adsorption of water causes the conversion of Lewis to Brønsted acid sites [44,45]. Thus, we hypothesized that the water released during the formation of the pyrrole ring plays a key role in the acidity of CATAPAL 200 and the mechanism mediated by the energetically preferred pyrrolidine-2,5-diol [46].



Scheme 4. A plausible mechanism for the synthesis of *N*-substituted pyrroles **3** catalyzed by the commercially available CATAPAL 200.

In order to unequivocally confirm the formation of a pyrrole core, single crystals suitable for X-ray diffraction analysis were grown for compound **3g** in methanol, using the slow evaporation method at ambient temperature under normal atmospheric conditions. Although compound **3g** has been previously synthesized in our research group [39], the structural information obtained from the crystallographic analysis has not been reported until now. As a result, single crystal X-ray diffraction analysis was performed over suitable crystals of compound **3g**. Interestingly, as an achiral molecule, it crystallizes in a non-centrosymmetric space group. This phenomenon was already observed in (5-formylfuran-2-yl)methyl 4-chlorobenzoate and 2-oxo-2*H*-chromen-7-yl 4-chlorobenzoate [47,48]. The crystal data, data collection, and structure refinement information are summarized in Table S1. The molecular structure of compound **3g** drawn as ellipsoids (50% probability level) is shown in Figure 2a. The molecular conformation in the crystal is characterized by two planar fragments linked by a methylene group. The weighted least-square planes that contain the 4-chlorophenyl and 2,5-dimethylpyrrole rings have a dihedral angle of 87.1° (Figure 2b), making these fragments nearly orthogonal. Notably, the supramolecular assembly is dominated by weak interactions which explains the low melting point (58–59 °C). The shortest interactions are detected through C7–H7···Cl1i and C2–H2···Cl1ii (symmetry codes: (i) $1/2 - x, 1/2 + y, -z$; (ii) $1/2 + x, 1/2 + y, z$) contacts with H···Cl distances of 3.06 and 3.09 Å, respectively (Figure 2c) [49]. These contacts form molecular sheets stacked along [001] direction and connected between them by a combination of C3–H3···πiii (H···π distance of 2.55 Å; symmetry code: (iii) $3/2 - x, 1/2 + y, 1 - z$) and van der Waals interactions.

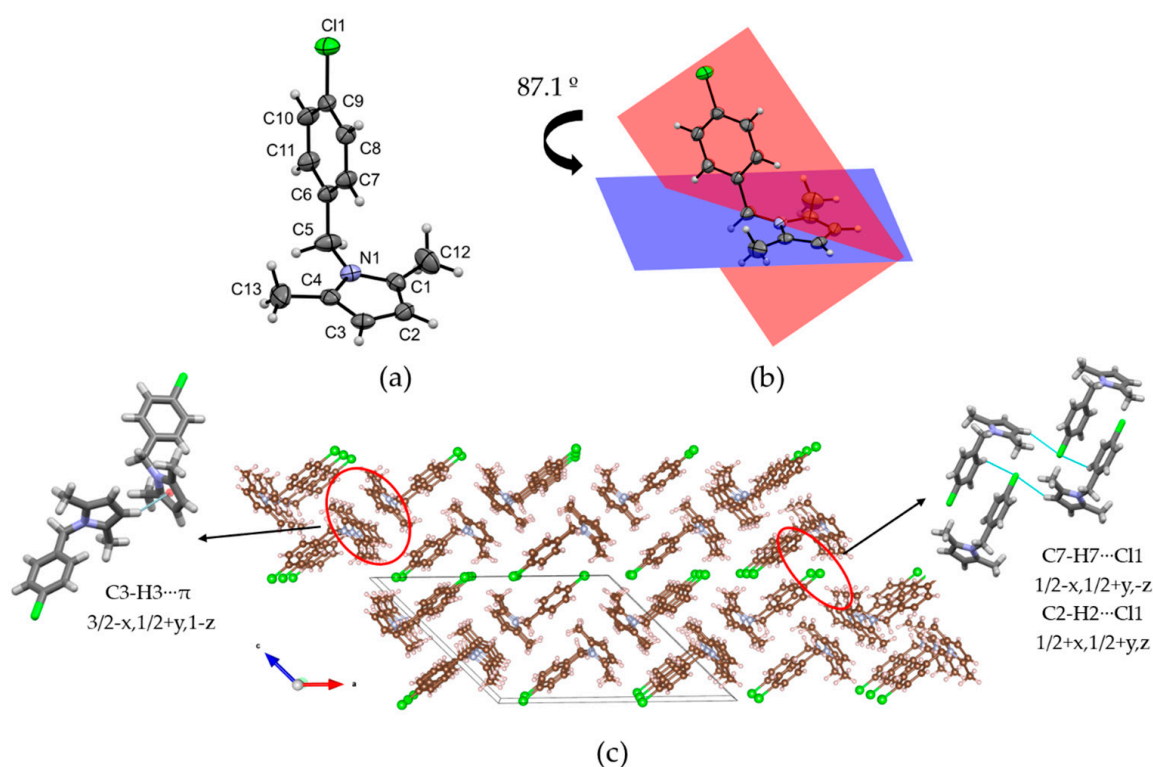


Figure 2. (a) Molecular structure of compound **3g** with anisotropic thermal vibration ellipsoids drawn at the 50% probability level. (b) The dihedral angle between planar fragments. (c) Packing of the compound **3g** showing the C–H...Cl and C–H... π interactions.

Hirshfeld surface analysis mapped over d_{norm} shows red spots over the centroid of the 2,5-dimethylpyrrole ring which suggests that the C3–H3... π contact is smaller than the sum of the van der Waals radii of the atoms involved (Figure 3a) [50]. However, an additional interaction highlighted as red spots are observed for C5–H5B...C3iv (H...C distance of 2.72 Å; symmetry code: (iv) $x, -1 + y, z$) (Figure 3b). In this interaction, the C3 atom has a negative partial charge ($C\delta^-$) due to the resonance effect in the pyrrole ring, while the H5B atom has a positive partial charge ($H\delta^+$) due to the electron-withdrawing groups connected to the methylene bridge (Figure 3b). This phenomenon is rare with scarce reports, mainly theoretical studies involving carbanions [51,52]. However, it is a case with experimental evidence. The observation of this interaction is probably due to the low-temperature measurement which allows the molecules to interact in this form. Figure 3 shows that nearly the entire Hirshfeld map is blue or white, which is due to the long interactions (equal or higher than the sum of the van der Waals radii) that control the crystal structure. Finally, the X-ray powder crystallographic data of compound **3g** is depicted in Supplementary Materials.

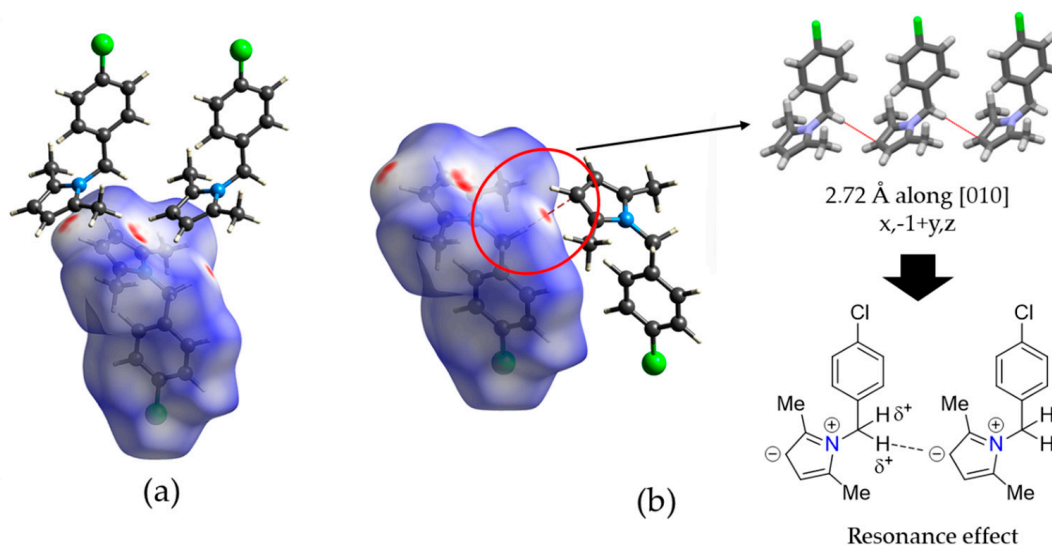


Figure 3. (a) Hirshfeld surface of compound **3g** mapped over d_{norm} showing the C–H \cdots π interactions highlighted with red spots. (b) Experimental evidence of interesting C–H \cdots C interactions showing the resonance effect that allows these contacts.

3. Materials and Methods

3.1. General Information

All reagents were purchased from Aldrich and used without further purification. The starting materials were weighed and handled in the air at ambient temperature. Catalysts were provided from SASOL Company (Houston, TX, USA) and treated at ambient temperature under vacuum for 4 h. They are CATAPAL 200, CATAPAL C-1, CATALOX Sba-90, and CATALOX SBA-200 (Sasol, Houston, TX, USA). The silica gel aluminum plates (Merck 60 F254, Darmstadt, Germany) were used for analytical TLC. Melting points were measured on Bs-448 apparatus (Bioamerican Science, Buenos Aires, Argentina). Pyrrole derivatives were purified by flash column chromatography using a mixture of *n*-hexane/ethyl acetate as an eluent. All compounds were identified by NMR data (Bruker BioSpin GmbH, Rheinstetten, Germany) with the previously reported data. NMR spectra were recorded at 400 and 500 MHz (^1H) and 101 and 125 MHz (^{13}C), respectively, at 298 K in CDCl_3 using as internal standards the residual non-deuterated signal for ^1H NMR and the deuterated solvent signal for $^{13}\text{C}\{^1\text{H}\}$ NMR spectroscopy. DEPT spectra (Bruker BioSpin GmbH, Rheinstetten, Germany) were used for the assignment of carbon signals. Chemical shifts (δ) are given in ppm and coupling constants (J) are given in Hz. The following abbreviations are used for multiplicity: s = singlet, d = doublet, t = triplet, and m = multiplet. The high-resolution mass spectra (HRMS) were recorded using a QTOF 5600 plus triple TOF spectrometer (Agilent Technologies Inc., Santa Clara, CA, USA) via electrospray ionization.

3.2. Catalyst Characterization

The X-ray diffraction patterns were recorded in PANalytical X'Pert Pro equipment (Malvern Panalytical, Almelo, The Netherlands) using CuK radiation ($L = 1.54056 \text{ \AA}$), in the 2θ range of $10\text{--}90^\circ$, with a count time of 1 s and a step size of $0.05^\circ \text{ s}^{-1}$. N_2 adsorption–desorption isotherms of solids were measured at 77 K in Micromeritics ASAP 2020 equipment (Micromeritics GmbH, Unterschleißheim, Germany). Samples were previously degassed at 100°C under vacuum for 18 h. The Brunauer–Emmett–Teller (BET) isotherm and Barrett, Joyner, and Halenda (BJH) method were used to calculate the specific surface area and pore volume. The nature of acid sites was studied by pyridine adsorption followed by FT-IR. Infrared spectra were collected using Nicolet iS50 equipment (Thermo Fisher Scientific, Waltham, MA, USA) with an in situ diffuse reflectance cell. In the same manner, the acid strength was determined by potentiometric titration using *n*-butylamine

(0.025 N) solution at a flow rate of 0.05 mL/min in 794 Basic Titrino Metrohm equipment (Metrohm AG, Herisau, Switzerland) using a double junction electrode.

3.3. X-ray Diffraction

The crystals of the compound **3g** were covered with a layer of a viscous perfluoropolyether (FomblinY) (Alfa Aesar, Tewksbury, MA, USA). A suitable crystal was selected with the aid of a microscope, mounted on a cryoloop, and placed in the low temperature nitrogen stream of the diffractometer. The intensity data sets were collected at 200 K on a Bruker AXS D8 Venture diffractometer (Bruker BioSpin GmbH, Rheinstetten, Germany) equipped with an Oxford Cryostream 700 unit (Oxford Cryosystems Ltd., Oxford, UK). Crystallographic data are presented in Table S1. The structure was solved using the WINGX package [53] by intrinsic phasing methods (SHELXT) [54] and refined by least-squares against F^2 (SHELXL-2014/7) [55]. All non-hydrogen atoms were anisotropically refined, whereas hydrogen atoms were included, positioned geometrically and refined by using a riding model (C–H: 0.95–0.99 Å). CCDC 2,239,500 contains the supplementary crystallographic data for this paper. These data can be obtained free of charge via <http://www.ccdc.cam.ac.uk/conts/retrieving.html> (or from the CCDC, 12 Union Road, Cambridge CB2 1EZ, UK; Fax: +44 1223 336033; E-mail: deposit@ccdc.cam.ac.uk).

3.4. Synthesis of Pyrrole Derivatives

A mixture of acetylacetone **1** (1 mmol), primary amine **2a–p** (1 mmol), and 40 mg of catalyst (CATAPAL 200) was heated at 60 °C for 45 min under solvent-free conditions. The progress of the reaction was followed by TLC using a mixture of *n*-hexane/ethyl acetate as an eluent. Then, desired compounds were extracted with ethyl acetate (2 × 5 mL), and the catalyst was separated by centrifugation and filtration. All synthesized compounds **3a–p** were purified by flash column chromatography using a mixture of *n*-hexane/ethyl acetate as an eluent. These compounds were identified by NMR data with the previously reported data.

3.4.1. 2,5-Dimethyl-1-phenyl-1H-pyrrole **3a**

The solvent-free reaction of acetylacetone **1** (118 µL, 1 mmol), aniline **2a** (91 µL, 1 mmol), and 40 mg of catalyst was heated at 60 °C for 45 min, affording compound **3a** as a brown solid (125 mg, 73%). M.p. 49 °C. ^1H NMR (500 MHz, CDCl_3): δ = 2.06 (s, 6H), 5.93 (s, 2H), 7.24 (d, J = 7.0 Hz, 2H), 7.42 (t, J = 7.5 Hz, 1H), 7.48 (t, J = 7.0 Hz, 2H) ppm. $^{13}\text{C}\{^1\text{H}\}$ NMR (125 MHz, CDCl_3): δ = 13.0, 105.7, 127.6, 128.3, 128.8, 129.0, 139.1 ppm. These NMR data matched previously reported data [56].

3.4.2. 2,5-Dimethyl-1-(*p*-tolyl)-1H-pyrrole **3b**

The solvent-free reaction of acetylacetone **1** (118 µL, 1 mmol), 4-methylaniline **2b** (107 mg, 1 mmol), and 40 mg of catalyst was heated at 60 °C for 45 min, affording compound **3b** as a brown solid (178 mg, 96%). M.p. 45–47 °C. ^1H NMR (400 MHz, CDCl_3): δ = 2.13 (s, 6H), 2.51 (s, 3H), 5.99 (s, 2H), 7.19 (d, J = 8.0 Hz, 2H), 7.34 (d, J = 8.0 Hz, 2H) ppm. $^{13}\text{C}\{^1\text{H}\}$ NMR (101 MHz, CDCl_3): δ = 13.1, 21.2, 105.5, 128.0, 128.8, 129.7, 136.4, 137.5 ppm. These NMR data matched previously reported data [57].

3.4.3. 1-(3-Methoxy-5-(trifluoromethyl)phenyl)-2,5-dimethyl-1H-pyrrole **3c**

The solvent-free reaction of acetylacetone **1** (118 µL, 1 mmol), 3-methoxy-5-(trifluoromethyl)aniline **2c** (191 mg, 1 mmol), and 40 mg of catalyst was heated at 60 °C for 45 min, affording compound **3c** as a yellow solid (223 mg, 83%). M.p. 76 °C. ^1H NMR (400 MHz, CDCl_3): δ = 2.07 (s, 6H), 3.88 (s, 3H), 5.93 (s, 2H), 6.95 (dd, J = 2.0, 2.0 Hz, 1H), 7.10 (s, 1H), 7.19 (s, 1H) ppm. $^{19}\text{F}\{^1\text{H}\}$ NMR (376 MHz, CDCl_3): δ = −62.8 (CF_3) ppm. $^{13}\text{C}\{^1\text{H}\}$ NMR (101 MHz, CDCl_3): δ = 13.1 (CH_3), 55.9 (CH_3), 106.6 (CH), 110.4 (CH, q, $^3J_{\text{C-F}}$ = 3.7 Hz), 117.5 (CH, q, $^3J_{\text{C-F}}$ = 3.7 Hz), 117.5 (CH) 123.7 (Cq, q, $^1J_{\text{C-F}}$ = 273.7 Hz),

128.8 (Cq), 132.6 (Cq, q, $^2J_{C-F} = 33.0$ Hz), 140.9 (Cq), 160.5 (Cq) ppm. HRMS (ESI+): calcd for $C_{14}H_{15}F_3NO^+$, 270.1100 [M + H] $^+$; found, 270.1092.

3.4.4. 1-(4-Chlorophenyl)-2,5-dimethyl-1H-pyrrole 3d

The solvent-free reaction of acetonylacetone **1** (118 μ L, 1 mmol), 4-chloroaniline **2d** (127 mg, 1 mmol), and 40 mg of catalyst was heated at 60 °C for 45 min, affording compound **3d** as a white solid (179 mg, 87%) after silica gel purification using EtOAc/*n*-hexane (1:20, *v/v*) as an eluent. M.p. 56–57 °C. 1H NMR (400 MHz, $CDCl_3$): $\delta = 2.04$ (s, 6H), 5.91 (s, 2H), 7.16 (d, $J = 8.4$ Hz, 2H), 7.44 (d, $J = 8.4$ Hz, 2H) ppm. $^{13}C\{^1H\}$ NMR (101 MHz, $CDCl_3$): $\delta = 13.1$ (CH₃), 106.2 (CH), 128.9 (Cq), 129.5 (CH), 129.6 (CH), 133.7 (Cq), 137.7 (Cq) ppm. HRMS (ESI+): calcd for $C_{12}H_{13}ClN^+$, 206.0731 [M + H] $^+$; found, 206.0723. These NMR data matched previously reported data [58].

3.4.5. 2,5-Dimethyl-1-(4-nitrophenyl)-1H-pyrrole 3e

The solvent-free reaction of acetonylacetone **1** (118 μ L, 1 mmol), 4-nitroaniline **2e** (138 mg, 1 mmol), and 40 mg of catalyst was heated at 60 °C for 45 min, affording compound **3e** as a red solid (166 mg, 77%). M.p. 148–149 °C. 1H NMR (500 MHz, $CDCl_3$): $\delta = 2.07$ (s, 6H), 5.96 (s, 2H), 7.39 (d, $J = 9.0$ Hz, 2H), 8.34 (d, $J = 9.0$ Hz, 2H) ppm. $^{13}C\{^1H\}$ NMR (125 MHz, $CDCl_3$): $\delta = 13.1$, 107.4, 124.2, 124.6, 128.8, 144.8, 146.8 ppm. These NMR data matched previously reported data [56].

3.4.6. 1-Benzyl-2,5-dimethyl-1H-pyrrole 3f

The solvent-free reaction of acetonylacetone **1** (118 μ L, 1 mmol), benzylamine **2f** (109 μ L, 1 mmol), and 40 mg of catalyst was heated at 60 °C for 45 min, affording compound **3f** as a white solid (180 mg, 97%). M.p. 44–45 °C. 1H NMR (400 MHz, $CDCl_3$): $\delta = 2.18$ (s, 6H), 5.04 (s, 2H), 5.90 (s, 2H), 6.92 (d, $J = 7.2$ Hz, 2H), 7.26 (t, $J = 7.4$ Hz, 1H), 7.33 (dd, $J = 7.4$, 7.4 Hz, 2H) ppm. $^{13}C\{^1H\}$ NMR (101 MHz, $CDCl_3$): $\delta = 12.6$ (CH₃), 46.8 (CH₂), 105.5 (CH), 125.8 (CH), 127.1 (CH), 128.1 (Cq), 128.8 (CH), 138.7 (Cq) ppm. HRMS (ESI+): calcd for $C_{13}H_{16}N^+$, 186.1277 [M + H] $^+$; found, 186.1271. These NMR data matched previously reported data [58].

3.4.7. 1-(4-Chlorobenzyl)-2,5-dimethyl-1H-pyrrole 3g

The solvent-free reaction of acetonylacetone **1** (118 μ L, 1 mmol), 4-chlorobenzylamine **2g** (122 μ L, 1 mmol), and 40 mg of catalyst was heated at 60 °C for 45 min, affording compound **3g** as a yellow pale solid (209 mg, 95%) after silica gel purification using CH_2Cl_2 /*n*-hexane (1:2, *v/v*) as an eluent. It should be noted that the compound **3g** was recrystallized in methanol as colorless prisms suitable for X-ray diffraction analysis and its crystallographic data were deposited in CSD with code CCDC 2239500. M.p. 58–59 °C. 1H NMR (400 MHz, $CDCl_3$): $\delta = 2.04$ (s, 6H), 4.89 (s, 2H), 5.78 (s, 2H), 6.72 (d, $J = 8.6$ Hz, 2H), 7.18 (d, $J = 8.6$ Hz, 2H) ppm. $^{13}C\{^1H\}$ NMR (101 MHz, $CDCl_3$): $\delta = 12.5$ (CH₃), 46.2 (CH₂), 105.8 (CH), 127.2 (CH), 128.0 (Cq), 129.0 (CH), 133.0 (Cq), 137.2 (Cq) ppm. HRMS (ESI+): calcd for $C_{13}H_{15}ClN^+$, 220.0888 [M + H] $^+$; found, 220.0877. These NMR data matched previously reported data [59].

3.4.8. 1-(3,5-bis(Trifluoromethyl)benzyl)-2,5-dimethyl-1H-pyrrole 3h

The solvent-free reaction of acetonylacetone **1** (118 μ L, 1 mmol), 3,5-bis(trifluoromethyl)benzylamine **2h** (243 mg, 1 mmol), and 40 mg of catalyst was heated at 60 °C for 45 min, affording compound **3h** as a white solid (292 mg, 91%) after silica gel purification using *n*-hexane as an eluent. M.p. 62 °C. 1H NMR (400 MHz, $CDCl_3$): $\delta = 2.13$ (s, 6H), 5.12 (s, 2H), 5.91 (s, 2H), 7.30 (s, 2H), 7.78 (s, 1H) ppm. $^{19}F\{^1H\}$ NMR (376 MHz, $CDCl_3$): $\delta = -62.9$ (CF₃) ppm. $^{13}C\{^1H\}$ NMR (101 MHz, $CDCl_3$): $\delta = 12.5$ (CH₃), 46.2 (CH₂), 106.7 (CH), 121.5 (CH, q, $^3J_{C-F} = 3.6$ Hz), 123.3 (Cq, q, $^1J_{C-F} = 273.8$ Hz), 126.0 (CH, q, $^3J_{C-F} = 3.1$ Hz), 127.7 (Cq), 132.4 (Cq, q, $^2J_{C-F} = 33.4$ Hz), 141.7 (Cq) ppm. HRMS (ESI+): calcd for $C_{15}H_{14}F_6N^+$, 322.1025 [M + H] $^+$; found, 322.1014.

3.4.9. 2,5-Dimethyl-1-(naphthalen-1-yl)-1H-pyrrole **3i**

The solvent-free reaction of acetonylacetone **1** (118 μ L, 1 mmol), naphthalen-1-amine **2i** (143 mg, 1 mmol), and 40 mg of catalyst was heated at 60 °C for 45 min, affording compound **3i** as a white solid (184 mg, 83%). M.p. 117–118 °C. ^1H NMR (400 MHz, CDCl_3): δ = 1.92 (s, 6H), 6.04 (s, 2H), 7.17 (d, J = 8.4 Hz, 1H), 7.43–7.49 (m, 2H), 7.52–7.60 (m, 2H), 7.94–7.96 (m, 2H) ppm. $^{13}\text{C}\{^1\text{H}\}$ NMR (101 MHz, CDCl_3): δ = 12.6, 105.4, 123.3, 125.4, 126.2, 126.5, 127.2, 128.0, 128.5, 129.9, 131.9, 134.2, 135.7 ppm. These NMR data matched previously reported data [58].

3.4.10. 1-Butyl-2,5-dimethyl-1H-pyrrole **3j**

The solvent-free reaction of acetonylacetone **1** (118 μ L, 1 mmol), *n*-butylamine **2j** (99 μ L, 1 mmol), and 40 mg of catalyst was heated at 60 °C for 45 min, affording compound **3j** as a yellow oil (136 mg, 90%). ^1H NMR (400 MHz, CDCl_3): δ = 0.98 (t, J = 7.2 Hz, 3H), 1.35–1.42 (m, 2H), 1.57–1.67 (m, 2H), 2.24 (s, 6H), 3.74 (t, J = 7.6 Hz, 2H), 5.78 (s, 2H) ppm. $^{13}\text{C}\{^1\text{H}\}$ NMR (101 MHz, CDCl_3): δ = 12.5, 13.9, 20.2, 33.2, 43.4, 104.9, 127.3 ppm. These NMR data matched previously reported data [60].

3.4.11. 2-(2,5-Dimethyl-1H-pyrrol-1-yl)aniline **3k**

The solvent-free reaction of acetonylacetone **1** (118 μ L, 1 mmol), *o*-phenylenediamine **2k** (108 mg, 1 mmol), and 40 mg of catalyst was heated at 60 °C for 45 min, affording compound **3k** as a yellow solid (164 mg, 88%). M.p. 70–71 °C. ^1H NMR (400 MHz, CDCl_3): δ = 1.98 (s, 6H), 3.43 (s, 2H, NH_2), 5.93 (s, 2H), 6.78–6.81 (m, 2H), 7.05 (dd, J = 7.8, 1.5 Hz, 1H), 7.20 (td, J = 7.8, 1.5 Hz, 1H) ppm. $^{13}\text{C}\{^1\text{H}\}$ NMR (101 MHz, CDCl_3): δ = 12.3, 105.8, 115.5, 118.2, 124.4, 128.4, 129.3, 129.3, 144.1 ppm. These NMR data matched previously reported data [61].

3.4.12. 2-(2,5-Dimethyl-1H-pyrrol-1-yl)benzo[d]thiazole **3l**

The solvent-free reaction of acetonylacetone **1** (118 μ L, 1 mmol), benzo[d]thiazol-2-amine **2l** (150 mg, 1 mmol), and 40 mg of catalyst was heated at 60 °C for 45 min, affording compound **3l** as a brown oil (201 mg, 88%). ^1H NMR (400 MHz, CDCl_3): δ = 2.35 (s, 6H), 5.97 (s, 2H), 7.47 (t, J = 7.8 Hz, 1H), 7.56 (t, J = 7.6 Hz, 1H), 7.90 (d, J = 8.0 Hz, 1H), 8.07 (d, J = 8.0 Hz, 1H) ppm. $^{13}\text{C}\{^1\text{H}\}$ NMR (101 MHz, CDCl_3): δ = 13.6, 108.6, 121.4, 123.4, 125.5, 126.5, 130.0, 135.1, 150.4, 158.6 ppm. These NMR data matched previously reported data [39].

3.4.13. 6-Chloro-2-(2,5-dimethyl-1H-pyrrol-1-yl)benzo[d]thiazole **3m**

The solvent-free reaction of acetonylacetone **1** (118 μ L, 1 mmol), 6-chlorobenzo[d]thiazol-2-amine **2m** (184 mg, 1 mmol), and 40 mg of catalyst was heated at 60 °C for 45 min, affording compound **3m** as a brown oil (210 mg, 80%). ^1H NMR (400 MHz, CDCl_3): δ = 2.36 (s, 6H), 5.98 (s, 2H), 7.51 (dd, J = 7.6, 1.5 Hz, 1H), 7.86 (d, J = 1.5 Hz, 1H), 7.96 (d, J = 7.6 Hz, 1H) ppm. $^{13}\text{C}\{^1\text{H}\}$ NMR (101 MHz, CDCl_3): δ = 13.7, 109.0, 121.0, 124.1, 127.3, 130.1, 131.4, 136.0, 148.9, 158.8 ppm. These NMR data matched previously reported data [39].

3.4.14. 2-(2,5-Dimethyl-1H-pyrrol-1-yl)-6-nitrobenzo[d]thiazole **3n**

The solvent-free reaction of acetonylacetone **1** (118 μ L, 1 mmol), 6-nitrobenzo[d]thiazol-2-amine **2n** (195 mg, 1 mmol), and 40 mg of catalyst was heated at 60 °C for 45 min, affording compound **3n** as a brown solid (191 mg, 70%). M.p. 125–127 °C. ^1H NMR (400 MHz, CDCl_3): δ = 2.45 (s, 6H), 6.01 (s, 2H), 8.10 (d, J = 7.5 Hz, 1H), 8.40 (dd, J = 7.5, 1.5 Hz, 1H), 8.82 (d, J = 1.5 Hz, 1H) ppm. $^{13}\text{C}\{^1\text{H}\}$ NMR (101 MHz, CDCl_3): δ = 13.8, 109.8, 117.3, 121.5, 122.6, 129.8, 134.0, 144.3, 153.8, 162.6 ppm. These NMR data matched previously reported data [39].

3.4.15. 5-(2,5-Dimethyl-1*H*-pyrrol-1-yl)-3-methyl-1-phenyl-1*H*-pyrazole **3o**

The solvent-free reaction of acetonylacetone **1** (118 μ L, 1 mmol), 3-methyl-1-phenyl-1*H*-pyrazol-5-amine **2o** (173 mg, 1 mmol), and 40 mg of catalyst was heated at 60 °C for 45 min, affording compound **3o** as a yellow oil (239 mg, 95%) after silica gel purification using EtOAc/*n*-hexane (1:20, *v/v*) as an eluent. ^1H NMR (400 MHz, CDCl_3): δ = 1.92 (s, 6H), 2.41 (s, 3H), 5.89 (s, 2H), 6.22 (s, 1H), 7.00 (dd, J = 1.4, 7.2 Hz, 2H), 7.19 (tt, J = 1.4, 7.2 Hz, 1H), 7.28 (t, J = 7.2 Hz, 2H) ppm. $^{13}\text{C}\{^1\text{H}\}$ NMR (101 MHz, CDCl_3): δ = 12.5 (CH_3), 14.4 (CH_3), 106.2 (CH), 107.5 (CH), 121.3 (CH), 126.7 (CH), 129.3 (CH), 129.3 (Cq), 136.5 (Cq), 138.9 (Cq), 149.3 (Cq) ppm. HRMS (ESI+): calcd for $\text{C}_{16}\text{H}_{18}\text{N}_3^+$, 252.1495 [M + H] $^+$; found, 252.1489.

3.4.16. 2-((2,5-Dimethyl-1*H*-pyrrol-1-yl)methyl)-1*H*-benzo[*d*]imidazole **3p**

The solvent-free reaction of acetonylacetone **1** (118 μ L, 1 mmol), (1*H*-benzo[*d*]imidazol-2-yl)methanamine **2p** (147 mg, 1 mmol), and 40 mg of catalyst was heated at 60 °C for 45 min, affording compound **3p** as a yellow solid (153 mg, 68%) after silica gel purification using EtOAc/*n*-hexane (1:4, *v/v*) as an eluent. M.p. 225 °C. ^1H NMR (400 MHz, CDCl_3): δ = 2.18 (s, 6H), 5.30 (s, 2H), 5.91 (s, 2H), 7.26 (dd, J = 3.0, 5.8 Hz, 2H), 7.53 (dd, J = 3.0, 5.8 Hz, 2H), 8.00 (br s, 1H, NH) ppm. $^{13}\text{C}\{^1\text{H}\}$ NMR (101 MHz, CDCl_3): δ = 12.5 (CH_3), 42.1 (CH_2), 107.1 (CH), 115.3 (CH), 123.2 (CH), 128.3 (Cq), 137.9 (Cq), 151.3 (Cq) ppm. HRMS (ESI+): calcd for $\text{C}_{14}\text{H}_{16}\text{N}_3^+$, 226.1339 [M + H] $^+$; found, 226.1332.

4. Conclusions

In summary, we have synthesized a wide range of *N*-substituted pyrroles through a Paal-Knorr reaction of acetonylacetone with primary amines under conventional heating at 60 °C for 45 min catalyzed by CATAPAL 200. Interestingly, the presence of rich Brønsted acid sites can accelerate the reaction to yield *N*-substituted pyrroles in good yields (68–97%) and selectivity close to 100%. This protocol is distinguished by its operational simplicity, high yields, reduced reaction time, no solvent required, stoichiometric amounts of reactants, low catalyst loading, and clean reaction profile. In addition, the catalyst is cheap and commercially available leading to an efficient and lower-cost chemical transformation. Remarkably, the catalyst is easily separated from the reaction medium and reused up to five times without appreciable loss of its catalytic activity. The use of supported aluminas in the sustainable synthesis of bioactive *N*-heterocycles and biomass valorization is currently in progress in our laboratory.

Supplementary Materials: The following supporting information can be downloaded at: <https://www.mdpi.com/article/10.3390/catal13030603/s1>. Figure S1: ^1H and $^{13}\text{C}\{^1\text{H}\}$ spectra for 2,5-dimethyl-1-phenyl-1*H*-pyrrole **3a**, Figure S2: ^1H and $^{13}\text{C}\{^1\text{H}\}$ spectra for 2,5-dimethyl-1-(*p*-tolyl)-1*H*-pyrrole **3b**, Figure S3: ^1H , $^{19}\text{F}\{^1\text{H}\}$, $^{13}\text{C}\{^1\text{H}\}$, and DEPT-135 spectra for 1-(3-methoxy-5-(trifluoromethyl)phenyl)-2,5-dimethyl-1*H*-pyrrole **3c**, Figure S4: ^1H , $^{13}\text{C}\{^1\text{H}\}$, and DEPT-135 spectra for 1-(4-chlorophenyl)-2,5-dimethyl-1*H*-pyrrole **3d**, Figure S5: ^1H and $^{13}\text{C}\{^1\text{H}\}$ spectra for 2,5-dimethyl-1-(4-nitrophenyl)-1*H*-pyrrole **3e**, Figure S6: ^1H , $^{13}\text{C}\{^1\text{H}\}$, and DEPT-135 spectra for 1-benzyl-2,5-dimethyl-1*H*-pyrrole **3f**, Figure S7: ^1H , $^{13}\text{C}\{^1\text{H}\}$, and DEPT-135 spectra for 1-(4-chlorobenzyl)-2,5-dimethyl-1*H*-pyrrole **3g**, Figure S8: ^1H , $^{19}\text{F}\{^1\text{H}\}$, $^{13}\text{C}\{^1\text{H}\}$, and DEPT-135 spectra for 1-(3,5-bis(trifluoromethyl)benzyl)-2,5-dimethyl-1*H*-pyrrole **3h**, Figure S9: ^1H and $^{13}\text{C}\{^1\text{H}\}$ spectra for 2,5-dimethyl-1-(naphthalen-1-yl)-1*H*-pyrrole **3i**, Figure S10: ^1H and $^{13}\text{C}\{^1\text{H}\}$ spectra for 2-(2,5-dimethyl-1*H*-pyrrol-1-yl)benzo[*d*]thiazole **3l**, Figure S11: ^1H and $^{13}\text{C}\{^1\text{H}\}$ spectra for 6-chloro-2-(2,5-dimethyl-1*H*-pyrrol-1-yl)benzo[*d*]thiazole **3m**, Figure S12: ^1H and $^{13}\text{C}\{^1\text{H}\}$ spectra for 2-(2,5-dimethyl-1*H*-pyrrol-1-yl)-6-nitrobenzo[*d*]thiazole **3n**, Figure S13: ^1H , $^{13}\text{C}\{^1\text{H}\}$, and DEPT-135 spectra for 5-(2,5-dimethyl-1*H*-pyrrol-1-yl)-3-methyl-1-phenyl-1*H*-pyrazole **3o**, Figure S14: ^1H , $^{13}\text{C}\{^1\text{H}\}$, DEPT-135, and HSQC spectra for 2-((2,5-dimethyl-1*H*-pyrrol-1-yl)methyl)-1*H*-benzo[*d*]imidazole **3p**, Figure S15: HRMS spectrum for 1-(3-methoxy-5-(trifluoromethyl)phenyl)-2,5-dimethyl-1*H*-pyrrole **3c**, Figure S16: HRMS spectrum for 1-(4-chlorophenyl)-2,5-dimethyl-1*H*-pyrrole **3d**, Figure S17: HRMS spectrum for 1-benzyl-2,5-dimethyl-1*H*-pyrrole **3f**, Figure S18: HRMS spectrum for 1-(4-chlorobenzyl)-2,5-dimethyl-1*H*-pyrrole **3g**, Figure S19: HRMS spectrum for 1-(3,5-bis(trifluoromethyl)benzyl)-2,5-dimethyl-1*H*-pyrrole **3h**, Figure S20: HRMS spec-

trum for 5-(2,5-dimethyl-1H-pyrrol-1-yl)-3-methyl-1-phenyl-1H-pyrazole **3o**, Figure S21: HRMS spectrum for 2-((2,5-dimethyl-1H-pyrrol-1-yl)methyl)-1H-benzo[d]imidazole **3p**, Figure S22: X-ray powder diffraction data for compound **3g**. Table S1: Experimental data for X-ray diffraction analysis for compound **3g**, Table S2: Surface area, pore volume, and pore size of CATAPAL 200, Table S3: Surface area, pore volume, and pore size of CATAPAL C-1, Table S4: Surface area, pore volume, and pore size of CATALOX SBA-90, Table S5: Surface area, pore volume, and pore size of CATALOX SBA-200.

Author Contributions: Investigation, data curation, writing—original draft preparation, O.P.-Z.; investigation, data curation, Ó.M.B.-A.; data curation, writing—original draft preparation, J.J.M.; writing—review and editing, H.R.; data curation, writing—original draft preparation, M.A.M.; writing—review and editing, I.I.; data curation, writing—original draft preparation, A.P.-R.; conceptualization, writing—original draft preparation, Á.S.; investigation, data curation, writing—original draft preparation, J.-C.C.; conceptualization, writing—original draft preparation, G.P.R. All authors have read and agreed to the published version of the manuscript.

Funding: This work was supported by the Consejo Nacional de Investigaciones Científicas y Técnicas CONICET (Funding number: PIP 0111).

Data Availability Statement: The data presented in this study are available in this article.

Acknowledgments: O.P.-Z., Á.S. and G.P.R. are grateful to Consejo Nacional de Investigaciones Científicas y Técnicas (CONICET) and Universidad Nacional de la Plata for financial support. J.J.M., H.R., and J.-C.C. acknowledge Universidad Pedagógica y Tecnológica de Colombia for financial support. M.A.M. acknowledges support from the Facultad de Ciencias at the Universidad de los Andes (FAPA-P18.160422.043). In addition, Ó.M.B.-A., I.I., and A.P.-R. thank Universidad de Alcalá for financial support. J.-C.C. also thanks to the program “Giner de los Ríos” at the Universidad de Alcalá. Finally, we are grateful to SASOL Company that kindly provided the aluminas used in this study.

Conflicts of Interest: The authors declare no conflict of interest.

References

1. Bhardwaj, V.; Gumber, D.; Abbot, V.; Dhiman, S.; Sharma, P. Pyrrole: A resourceful small molecule in key medicinal heteroaromatics. *RSC Adv.* **2015**, *5*, 15233–15266. [[CrossRef](#)]
2. Petri, G.L.; Spanò, V.; Spatola, R.; Holl, R.; Raimondi, M.V.; Barraja, P.; Montalbano, A. Bioactive pyrrole-based compounds with target selectivity. *Eur. J. Med. Chem.* **2020**, *208*, 112783. [[CrossRef](#)] [[PubMed](#)]
3. Dias Bianco, M.C.A.; Firmino Marinho, D.I.L.; Hoelz, L.V.; Macedo Bastos, M.; Boechat, N. Pyrroles as privileged scaffolds in the search for new potential HIV inhibitors. *Pharmaceuticals* **2021**, *14*, 893. [[CrossRef](#)] [[PubMed](#)]
4. Iqbal, S.; Rasheed, H.; Awan, R.J.; Awan, R.J.; Mukhtar, A.; Moloney, M.G. Recent advances in the synthesis of pyrroles. *Curr. Org. Chem.* **2020**, *24*, 1196–1229. [[CrossRef](#)]
5. Buckley, M.M.; Brogden, R.N. Ketorolac—A review of its pharmacodynamic and pharmacokinetic properties, and therapeutic potential. *Drugs* **1990**, *39*, 86–109. [[CrossRef](#)]
6. Moran, M.; Nickens, D.; Adcock, K.; Bennetts, M.; Desscan, A.; Charnley, N.; Fife, K. Sunitinib for metastatic renal cell carcinoma: A systematic review and meta-analysis of real-world and clinical trials data. *Target Oncol.* **2019**, *14*, 405–416. [[CrossRef](#)]
7. Lea, A.P.; McTavish, D. Atorvastatin—A review of its pharmacology and therapeutic potential in the management of hyperlipidaemias. *Drugs* **1997**, *53*, 828–847. [[CrossRef](#)]
8. Eastman, R.T.; Roth, J.S.; Brimacombe, K.R.; Simeonov, A.; Shen, M.; Patnaik, S.; Hall, M.D. Remdesivir: A review of its discovery and development leading to emergency use authorization for treatment of COVID-19. *ACS Cent. Sci.* **2020**, *6*, 672–683. [[CrossRef](#)]
9. Insuasty, D.; Castillo, J.; Becerra, D.; Rojas, H.; Abonia, R. Synthesis of biologically active molecules through multicomponent reactions. *Molecules* **2020**, *25*, 505. [[CrossRef](#)]
10. Estévez, V.; Villacampa, M.; Menéndez, J.C. Recent advances in the synthesis of pyrroles by multicomponent reactions. *Chem. Soc. Rev.* **2014**, *43*, 4633–4657. [[CrossRef](#)]
11. Motati, D.R.; Uredi, D.; Watkins, E.B. The discovery and development of oxalamide and pyrrole small molecule inhibitors of gp120 and HIV entry—A review. *Curr. Top. Med. Chem.* **2019**, *19*, 1650–1675. [[CrossRef](#)] [[PubMed](#)]
12. Philkhana, S.C.; Badmus, F.O.; Dos Reis, I.C.; Kartika, R. Recent advancements in pyrrole synthesis. *Synthesis* **2021**, *53*, 1531–1555. [[CrossRef](#)] [[PubMed](#)]
13. Leonardi, M.; Estévez, V.; Villacampa, M.; Menéndez, J.C. The Hantzsch pyrrole synthesis: Non-conventional variations and applications of a neglected classical reaction. *Synthesis* **2019**, *51*, 816–828. [[CrossRef](#)]
14. Magnus, N.A.; Staszak, M.A.; Udodong, U.E.; Wepsiec, J.P. Synthesis of 4-cyano pyrroles via mild Knorr reactions with β -ketonitriles. *Org. Process Res. Dev.* **2006**, *10*, 899–904. [[CrossRef](#)]

15. Balakrishna, A.; Aguiar, A.; Sobral, P.J.M.; Wani, M.Y.; Silva, J.A.; Sobral, A.J.F.N. Paal-Knorr synthesis of pyrroles: From conventional to green synthesis. *Catal. Rev.* **2019**, *61*, 84–110. [[CrossRef](#)]
16. Cheng, P.; Shao, W.; Clive, D.L.J. A general route to 1,3'-bipyrroles. *J. Org. Chem.* **2013**, *78*, 11860–11873. [[CrossRef](#)]
17. Zhang, L.; Zhang, J.; Ma, J.; Cheng, D.-J.; Tan, B. Highly atroposelective synthesis of arylpyrroles by catalytic asymmetric Paal-Knorr Reaction. *J. Am. Chem. Soc.* **2017**, *139*, 1714–1717. [[CrossRef](#)]
18. Luo, H.; Kang, Y.; Li, Q.; Yang, L. Sulfamic acid as efficient and reusable catalytic system for the synthesis of pyrrole, furan, and thiophene derivatives. *Heteroat. Chem.* **2008**, *19*, 144–148. [[CrossRef](#)]
19. Bharadwaj, A.R.; Scheidt, K.A. Catalytic multicomponent synthesis of highly substituted pyrroles utilizing a one-pot Sila-stetter/Paal-Knorr Strategy. *Org. Lett.* **2004**, *6*, 2465–2468. [[CrossRef](#)]
20. Török, B.; Schäfer, C.; Kokel, A. Chapter 3.8. Ring transformations by heterogeneous catalysis. In *Heterogeneous Catalysis in Sustainable Synthesis*, 1st ed.; Török, B., Schäfer, C., Kokel, A., Eds.; Elsevier: Amsterdam, The Netherlands, 2021; pp. 491–542. [[CrossRef](#)]
21. Azizi, N.; Khajeh-Amiri, A.; Ghafuri, H. Iron-catalyzed inexpensive and practical synthesis of *N*-substituted pyrroles in water. *Synlett* **2009**, *20*, 2245–2248. [[CrossRef](#)]
22. Aghapoor, K.; Mohsenzadeh, F.; Darabi, H.R.; Rastgar, S. Microwave-induced calcium(II) chloride-catalyzed Paal-Knorr pyrrole synthesis: A safe, expeditious, and sustainable protocol. *Res. Chem. Intermed.* **2018**, *44*, 4063–4072. [[CrossRef](#)]
23. De, S.K. Ruthenium (III) chloride as a novel and efficient catalyst for the synthesis of substituted pyrroles under solvent-free conditions. *Catal. Lett.* **2008**, *124*, 174–177. [[CrossRef](#)]
24. De, S.K. Cobalt(II) chloride as a novel and efficient catalyst for the synthesis of 1,2,5-trisubstituted pyrroles under solvent-free conditions. *Heteroat. Chem.* **2008**, *19*, 592–595. [[CrossRef](#)]
25. Chen, J.-X.; Liu, M.-C.; Yang, X.-L.; Ding, J.-C.; Wu, H.-Y. Indium(III)-catalyzed synthesis of *N*-substituted pyrroles under solvent-free conditions. *J. Braz. Chem. Soc.* **2008**, *19*, 877–883. [[CrossRef](#)]
26. Zhang, Z.-H.; Li, J.-J.; Li, T.-S. Ultrasound-assisted synthesis of pyrroles catalyzed by zirconium chloride under solvent-free conditions. *Ultrason. Sonochem.* **2008**, *15*, 673–676. [[CrossRef](#)]
27. Rahmatpour, A. ZrOCl₂·8H₂O as a highly efficient, eco-friendly and recyclable Lewis acid catalyst for one-pot synthesis of *N*-substituted pyrroles under solvent-free conditions at room temperature. *Appl. Organometal. Chem.* **2011**, *25*, 585–590. [[CrossRef](#)]
28. Srinivas, R.; Thirupathi, B.; Kumar, J.K.P.; Prasad, A.N.; Reddy, B.M. One-step synthesis of 1,2,5-trisubstituted pyrroles by copper catalyzed condensation of 1,4-diones with primary amines. *Curr. Org. Chem.* **2012**, *16*, 2482–2489. [[CrossRef](#)]
29. Li, P.; Weng, G.; Zhang, Y.; Zhang, X. A highly efficient Paal-Knorr synthesis of chiral pyrrole derivatives catalyzed by MgI₂. *Chin. J. Org. Chem.* **2016**, *36*, 364–369. [[CrossRef](#)]
30. Rahmatpour, A.; Aalaie, J. One-pot synthesis of *N*-substituted pyrroles catalyzed by polystyrene-supported aluminum chloride as a reusable heterogeneous Lewis acid catalyst. *Heteroat. Chem.* **2011**, *22*, 85–90. [[CrossRef](#)]
31. Rahmatpour, A. Polystyrene-supported GaCl₃ as a highly efficient and recyclable heterogeneous Lewis acid catalyst for one-pot synthesis of *N*-substituted pyrroles. *J. Organomet. Chem.* **2012**, *712*, 15–19. [[CrossRef](#)]
32. Aghapoor, K.; Ebadi-Nia, L.; Mohsenzadeh, F.; Morad, M.M.; Balavar, Y.; Darabi, H.R. Silica-supported bismuth(III) chloride as a new recyclable heterogeneous catalyst for the Paal-Knorr pyrrole synthesis. *J. Organomet. Chem.* **2012**, *708*, 25–30. [[CrossRef](#)]
33. Darabi, H.R.; Poorheravi, M.R.; Aghapoor, K.; Mirzaee, A.; Mohsenzadeh, F.; Asadollahnejad, N.; Taherzadeh, H.; Balavar, Y. Silica-supported antimony(III) chloride as a mild and reusable catalyst for the Paal-Knorr pyrrole synthesis. *Environ. Chem. Lett.* **2012**, *10*, 5–12. [[CrossRef](#)]
34. Aghapoor, K.; Amini, M.M.; Jadidi, K.; Mohsenzadeh, F.; Darabi, H.R. Catalytic activity of the nanoporous MCM-41 surface for the Paal-Knorr pyrrole cyclocondensation. *Z. Naturforsch.* **2015**, *70*, 475–481. [[CrossRef](#)]
35. Liu, L.; Corma, A. Metal catalysts for heterogeneous catalysis: From single atoms to nanoclusters and nanoparticles. *Chem. Rev.* **2018**, *118*, 4981–5079. [[CrossRef](#)] [[PubMed](#)]
36. Trueba, M.; Trasatti, S.P. γ -Alumina as a support for catalysts: A review of fundamental aspects. *Eur. J. Inorg. Chem.* **2005**, *2005*, 3393–3403. [[CrossRef](#)]
37. Clark, P.D.; Dowling, N.I.; Huang, M.; Okemona, O.; Butlin, G.D.; Hou, R.; Kijlstra, W.S. Studies on sulfate formation during the conversion of H₂S and SO₂ to sulfur over activated alumina. *Appl. Catal. A Gen.* **2002**, *235*, 61–69. [[CrossRef](#)]
38. Phung, T.K.; Herrera, C.; Larrubia, M.A.; García-Diéguez, M.; Finocchio, E.; Alemany, L.J.; Busca, G. Surface and catalytic properties of some γ -Al₂O₃ powders. *Appl. Catal. A Gen.* **2014**, *483*, 41–51. [[CrossRef](#)]
39. Portilla-Zúñiga, O.; Sathicq, Á.; Martínez, J.; Rojas, H.; De Geronimo, E.; Luque, R.; Romanelli, G.P. Novel bifunctional mesoporous catalysts based on Preyssler heteropolyacids for green pyrrole derivative synthesis. *Catalysts* **2018**, *8*, 419. [[CrossRef](#)]
40. Guthrie, J.P.; Guo, J. Intramolecular aldol condensations: Rate and equilibrium constants. *J. Am. Chem. Soc.* **1996**, *118*, 11472–11487. [[CrossRef](#)]
41. Pittman, C.U.; Liang, Y.F. Sequential catalytic condensation-hydrogenation of ketones. *J. Org. Chem.* **1980**, *45*, 5048–5052. [[CrossRef](#)]
42. Qian, K.; Tomczak, D.C.; Rakiewicz, E.F.; Harding, R.H.; Yaluris, G.; Cheng, Zhao, X.; Peters, A.W. Coke formation in the fluid catalytic cracking process by combined analytical techniques. *Energ. Fuels* **1997**, *11*, 596–601. [[CrossRef](#)]
43. Feng, R.; Bai, P.; Liu, S.; Zhang, P.; Liu, X.; Yan, Z.; Zhang, Z.; Gao, X. The application of mesoporous alumina with rich Brønsted acidic sites in FCC catalysts. *Appl. Petrochem. Res.* **2014**, *4*, 367–372. [[CrossRef](#)]

44. Cant, N.; Little, L. Lewis and Brønsted acid sites on silica-alumina. *Nature* **1966**, *211*, 69–70. [[CrossRef](#)]
45. Coster, D.; Blumenfeld, A.L.; Fripiat, J.J. Lewis acid sites and surface aluminum in aluminas and zeolites: A high-resolution NMR study. *J. Phys. Chem.* **1994**, *98*, 6201–6211. [[CrossRef](#)]
46. Abbat, S.; Dhaked, D.; Arfeen, M.; Bharatam, P.V. Mechanism of the Paal-Knorr reaction: The importance of water mediated hemiacetal pathway. *RSC Adv.* **2015**, *5*, 88353–88366. [[CrossRef](#)]
47. Castillo, J.C.; Martínez, J.J.; Becerra, D.; Rojas, H.; Macías, M.A. Obtaining (5-formylfuran-2-yl)methyl 4-chlorobenzoate through an esterification of 5-hydroxymethylfurfural: Interesting achiral molecule crystallizing in a Sohncke P₂₁2₁2₁ space group. *J. Mol. Struct.* **2022**, *1268*, 133713. [[CrossRef](#)]
48. Salinas-Torres, A.; Jiménez, E.; Becerra, D.; Martínez, J.J.; Rojas, H.; Castillo, J.-C.; Macías, M.A. Synthesis, anticancer evaluation, thermal and X-ray crystallographic analysis of 2-oxo-2H-chromen-7-yl 4-chlorobenzoate using a conductively heated sealed-vessel reactor. *J. Mol. Struct.* **2022**, *1274*, 134414. [[CrossRef](#)]
49. Desiraju, G.R.; Parthasarathy, R. The nature of halogen-halogen interactions: Are short halogen contacts due to specific attractive forces or due to close packing of nonspherical atoms? *J. Am. Chem. Soc.* **1989**, *111*, 8725–8726. [[CrossRef](#)]
50. Spackman, M.A.; Jayatilaka, D. Hirshfeld surface analysis. *CrystEngComm* **2009**, *11*, 19–32. [[CrossRef](#)]
51. Platts, J.A.; Howard, S.T.; Woźniak, K. Quantum chemical evidence for C–H···C hydrogen bonding. *Chem. Commun.* **1996**, 63–64. [[CrossRef](#)]
52. Chandra, A.K.; Zeegers-Huyskens, T. Theoretical study of (CH···C)-hydrogen bonds in CH₄-nXn (X = F, Cl; n = 0, 1, 2) systems complexed with their homoconjugate and heteroconjugate carbanions. *J. Phys. Chem. A* **2005**, *109*, 12006–12013. [[CrossRef](#)]
53. Farrugia, L.J. WinGX and ORTEP for Windows: An update. *J. Appl. Crystallogr.* **2012**, *45*, 849–854. [[CrossRef](#)]
54. Sheldrick, G.M. SHELXT-integrated space-group and crystal-structure determination. *Acta Crystallogr. Sect. A* **2015**, *71*, 3–8. [[CrossRef](#)]
55. Sheldrick, G.M. Crystal structure refinement with SHELXL. *Acta Crystallogr. Sect. C* **2015**, *71*, 3–8. [[CrossRef](#)] [[PubMed](#)]
56. Walia, A.; Kang, S.; Silverman, R.B. Microwave-assisted protection of primary amines as 2,5-dimethylpyrroles and their orthogonal deprotection. *J. Org. Chem.* **2013**, *78*, 10931–10937. [[CrossRef](#)]
57. Ibrahim, Y.A.; Li, J.; Ai, L.; Li, B. A convenient approach for the synthesis of substituted pyrroles by using phosphoric acid as a catalyst and their photophysical properties. *J. Mol. Struct.* **2022**, *1252*, 132123. [[CrossRef](#)]
58. Chen, X.; Yang, M.; Zhou, M. Efficient synthesis of substituted pyrroles through Pd(OCOFCF₃)₂-catalyzed reaction of 5-hexen-2-one with primary amines. *Tetrahedron Lett.* **2016**, *57*, 5215–5218. [[CrossRef](#)]
59. Fu, W.; Zhu, L.; Tan, S.; Zhao, Z.; Yu, X.; Wang, L. Copper/nitroxyl-catalyzed synthesis of pyrroles by oxidative coupling of diols and primary amines at room temperature. *J. Org. Chem.* **2022**, *87*, 13389–13395. [[CrossRef](#)]
60. Liu, Y.; Hu, Y.L. Novel and highly efficient preparation of pyrroles using supported ionic liquid ILCF₃SO₃@SiO₂ as a heterogeneous catalyst. *J. Iran. Chem. Soc.* **2018**, *15*, 1033–1040. [[CrossRef](#)]
61. Joshi, S.D.; Dixit, S.R.; Kirankumar, M.N.; Aminabhavi, T.M.; Raju, K.V.S.N.; Narayan, R.; Lherbet, C.; Yang, K.S. Synthesis, antimycobacterial screening and ligand-based molecular docking studies on novel pyrrole derivatives bearing pyrazoline, isoxazole and phenyl thiourea moieties. *Eur. J. Med. Chem.* **2016**, *107*, 133–152. [[CrossRef](#)]

Disclaimer/Publisher's Note: The statements, opinions and data contained in all publications are solely those of the individual author(s) and contributor(s) and not of MDPI and/or the editor(s). MDPI and/or the editor(s) disclaim responsibility for any injury to people or property resulting from any ideas, methods, instructions or products referred to in the content.